NPL REPORT DEPC-EM 001

Design of a bi-directional electrostatic actuator for realising nanonewton to micronewton forces

Richard K Leach & Simon Oldfield

Division of Engineering & Process Control

Shakil A Awan, John Blackburn & Jonathan M Williams

Division of Enabling Metrology

August 2004

Design of a bi-directional electrostatic actuator for realising nanonewton to micronewton forces

Richard K Leach & Simon Oldfield
Division of Engineering & Process Control

Shakil A Awan, John Blackburn & Jonathan M Williams
Division of Enabling Metrology

ABSTRACT

This report describes the design of an electrostatic actuator for incorporation into a low force measuring instrument that operates over the range 1 nN to 10 μN. The force being measured is balanced by applying an equal and opposite electrostatic restoring force. The low force measuring instrument also requires a prior calibration of the capacitance gradient of the actuator. A number of capacitor geometries were considered but the need for a bi-directional actuator and ease of manufacture have led to a system with two sets of parallel plate capacitors (*i.e.* a four-plate capacitor) with a moving dielectric plate that is displaced by the application of the force being measured. To the authors' knowledge such a four-plate capacitor arrangement has not been used before and should give a significant improvement over existing low force measuring instruments. The report describes a theoretical model of the four-plate capacitor with moving dielectric. Finite element models that were used to investigate the effects of undesired motion of the dielectric plate are then described. Unlike a two-plate capacitor, a four-plate design requires at least six measurements to determine a capacitance matrix and these measurements are discussed. Finally, the practical realisation of a four-plate capacitor is considered.

© Crown Copyright 2004
Reproduced by Permission of the Controller of HMSO

ISSN 1744-0254

National Physical Laboratory
Queens Road, Teddington, Middlesex, TW11 0LW

No extracts from this report may be reproduced without the prior written consent of the Managing Director, National Physical Laboratory; if consent is given the source must be acknowledged and may not be used out of context.

Approved on behalf of the Managing Director, NPL
by Dr Jerry Benson, Head, Division of Engineering & Process Control

CONTENTS

FIGURE LEGENDS

TABLES

1 INTRODUCTION

As part of the 2002 – 2005 National Measurement System Programme for Length, the National Physical Laboratory, in collaboration with the University of Warwick, are developing a low force measurement device with a range of 1 µN to 1 nN and a resolution of 50 pN. In practice, however, the range must extend to 10 µN to allow direct comparison with 1 mg standard masses. Measurements from the instrument will also be compared with those from micro-fabricated transfer devices being developed at NPL (Cumpson *et al* 2003, Cumpson and Hedley 2003) and at the lower end of its range with radiation pressure. The range of application for the instrument can be found at http://www.dti.gov.uk/nms/prog/new/length.pdf on page 58 and a report into the design of the mechanics can be found elsewhere (Henselmans *et al* 2004).

The instrument has some parallels with a similar instrument being developed at the National Institute of Standards and Technology (NIST), in that it utilises a moving platen, the position of which is monitored interferometrically. The force to be measured is applied to the platen, which has a servo controlled restoring force applied to it to keep the position at a null (Pratt *et al* 2004). The aim of this report is to describe in detail the design of a novel restoring force system that has the potential to offer significant advantages over that produced at NIST, both in its functionality and its practical realisation.

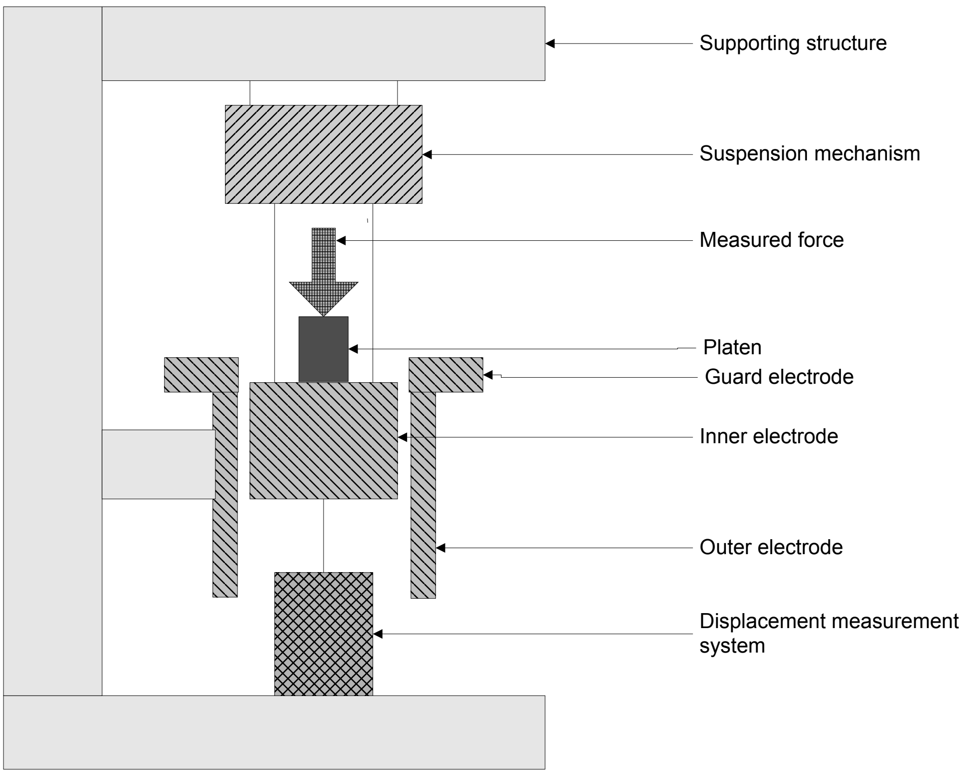

Figure 1 A low force balance, based on the original NIST design, showing the component parts

Figure 1 shows a schematic diagram of an instrument based on the original NIST design. Such an instrument requires the following sub-systems:

Platen. The force to be measured is applied to the platen in a way that is yet to be determined. If comparison with standard masses is to be undertaken, then the platen must be horizontal, with clear space above it. This arrangement would also be compatible with atomic force microscopes (AFMs) and other similar instruments. In order to be able to perform radiation pressure comparisons, the platen must have a reflectivity greater than 99%.

Restoring force system. It is intended that the force will be controlled by a servo system to be equal and opposite to the applied force. The magnitude of the restoring force must be capable of being calculated independently from easily measurable parameters that are traceable to Systeme International d'Unites.

Position sensor. As the force is applied to the platen it moves, its movement is sensed and used as the input to the servo control system. The resolution of the position sensor must be such that an applied force equal to the minimum force resolution required moves the platen by more than the position sensor resolution with no servo control mechanism operating.

Servo control system. As the platen starts to move, a servo control system is used to vary the restoring force such that the platen moves back to the null position. The servo system will be similar to that used for the horizontal force measurement balances that have been developed at NPL for measuring the thrust of ion engines for space applications (Hughes and Oldfield 2002).

Suspension and guidance system. The motion of the platen must be controlled so that only motion in the direction of application of the applied force is permitted. The stiffness of the suspension/guidance system must be sufficiently low such that a force equal to the minimum force to be resolved is capable of moving the platen a distance greater than the resolution of the position sensor.

Environmental isolation system. The instrument must be supported in such a way that it is sufficiently well isolated from external influences such as seismic and acoustic vibration, thermal gradients and air current. The isolation requirements of the proposed instrument are described elsewhere (Reilly and Leach 2004).

This report is chiefly concerned with describing the design of the restoring force mechanism. A novel type of four-plate capacitor design has been selected as the system of choice as it offers a number of benefits over existing systems.

2 DESIGN OF THE RESTORING FORCE SYSTEM

The restoring force applied to the platen must be equal and opposite to the force being measured. This implies, therefore, that the restoring force must be in the range 0 to 10 μN. Typically, small forces are applied either magnetically or electrostatically. Magnetic forces (for example, from a voice coil arrangement) are normally significantly higher in magnitude than the forces to be measured; so electrostatic actuation is more plausible. Electrostatic forces are generated by the application of voltage to a capacitor, the restoring force being in the direction of motion required to increase the capacitance (note that the capacitor acts as a 'full-wave rectifier' in that the force is always attractive, regardless of the polarity of the electrical supply). Additionally, the force must be capable of being calculated from readily measurable parameters, as no direct measure of force exists at this level. For a capacitor, the force, F, is given by

$$F = -\frac{1}{2}V^2\frac{dC}{dz}, \tag{2.1}$$

where dC/dz is the rate of change of capacitance per unit distance in the direction of motion and V is the applied voltage.

Two obvious capacitor geometries exist – either parallel plate, with the direction of force being at right angles to the plates, or overlapping cylinder, where the direction of force is along the cylinder axis (see Figures 2 and 3).

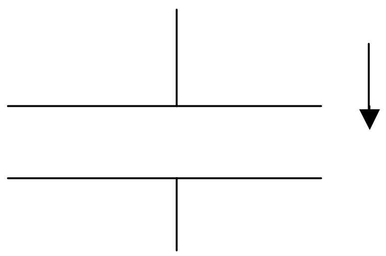

Figure 2 Parallel plate capacitor

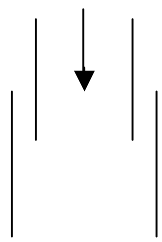

Figure 3 Cylindrical capacitor

In the above two geometries, the capacitance can be changed either by varying the gap/overlap distance, or by changing the dielectric constant of the space between the electrodes.

For the parallel plate configuration, the capacitance change is dependent on the plate separation, so the force per unit voltage changes as the plates move together - leading to a non-linear system. In the case of coaxial overlapping cylinders, suitable design can make the capacitance change approximately constant with changing overlap and small with respect to radial misalignment. This would appear to be the more suitable arrangement as the rate of change of capacitance with overlap can then be measured accurately. However, a parallel plate capacitor with fixed plates, but with a moving dielectric material between the plates would produce a linear system (see Figure 4).

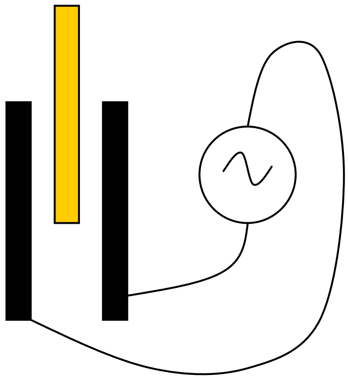

Figure 4 Parallel plate with moving dielectric

The two options for a concentric cylinder capacitor are a conducting cylinder moving relative to a fixed conducting cylinder (or between two fixed cylinders) – see figure 5 or a dielectric cylinder moving between two concentric conducting cylinders (see figure 6). The latter arrangement does not require any electrical connection to the moving cylinder, and would (with a suitable choice of dielectric) generate forces up to a factor of ten greater in magnitude, and so is to be preferred.

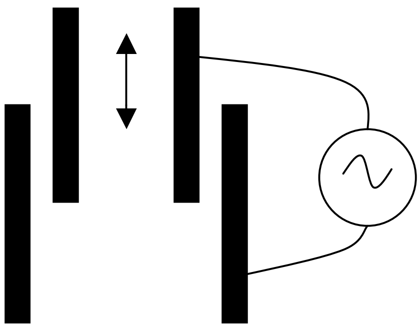

Figure 5 Moving conductor

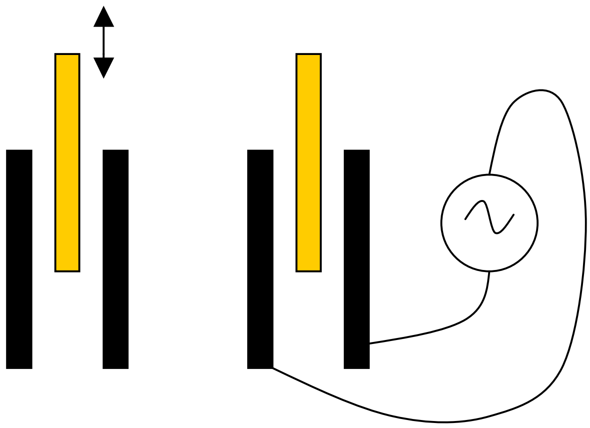

Figure 6 Moving dielectric

It should be noted that the capacitance of the above systems (and, therefore, the change in capacitance with separation) will vary if the gap between the electrodes changes (such as with thermal expansion), if the moving element moves away from the centre position (though suitable design should minimise this effect) or if the relative permittivity of the moving dielectric changes (such as with temperature, or humidity).

Independent measurement of the capacitance of the system is required, at a number of positions of the platen, in order to calculate the value of dC/dz. Measurement of capacitance is required to at least 1 in 10^5 in order that the required force uncertainty can be achieved.

The cylindrical design has the advantage of symmetry and a (relatively) small diameter of cylinder. However, very good surface finish is required on both of the conducting cylinders (one internal cylindrical surface and one external) and on the dielectric (both internal and external), and this may be difficult to achieve. Additionally, the external conducting cylinder needs to be made in at least two, perhaps three or four, sections, separated by insulators. For the parallel plate version, the fabrication of the electrodes (and of the dielectric) is much easier, as all surfaces can be optically polished. Additionally, the conducting surfaces could be vacuum deposited coatings with several conducting sections being laid down on a single substrate. This would allow the use of a single surface, polished in a single operation, but electrically split into several regions. The use of a suitably configured and electrically connected four-plate capacitor system (the subject of the rest of this report and see Figure 7) also allows the electrostatic force to be applied in two opposing directions. This is a considerable advantage over a single direction system, especially when determining the capacitance gradient.

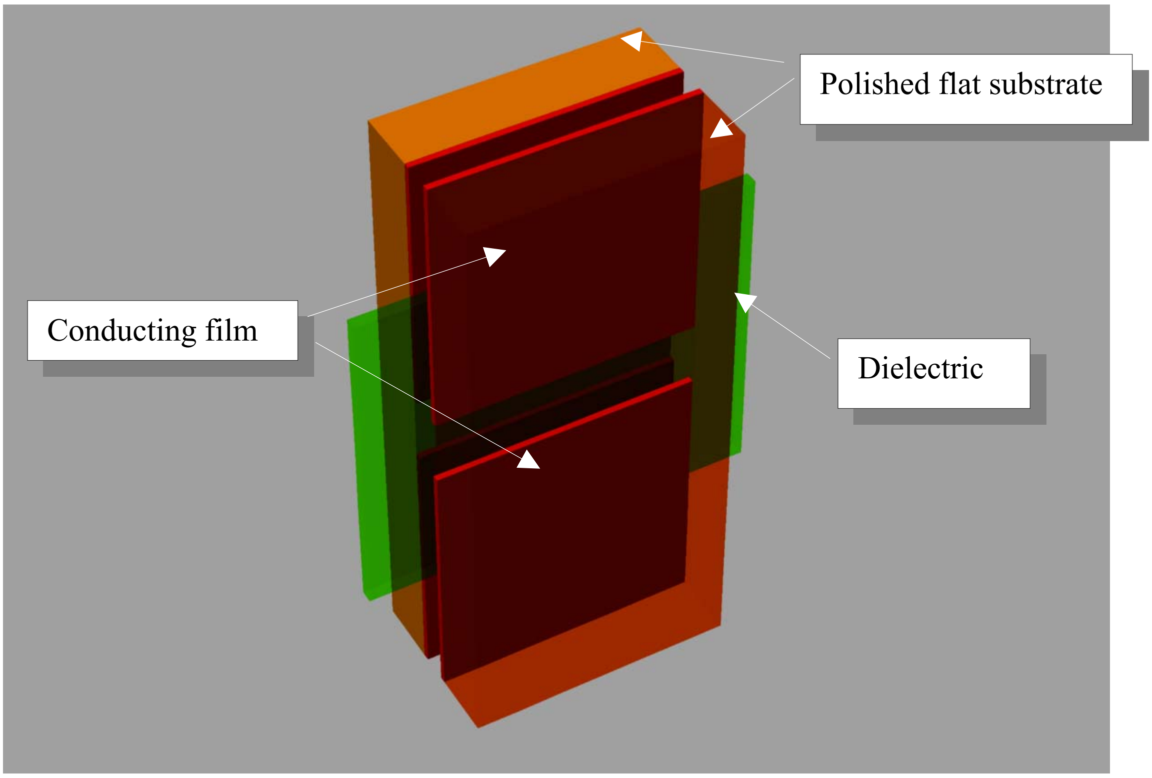

Figure 7 Schematic representation of a four-plate capacitor with moving dielectric

In summary, a four-plate capacitor system is relatively simple to manufacture and allows for bi-directional motion. However, as this is a novel design of capacitor a full theoretical analysis of the operation of the actuator was required. This analysis is the subject of §3, §4 and §5.

It is worth noting that the four-plate capacitor device that is being developed is essentially an implementation of equation (2.1) and requires the accurate determination of the applied voltage and the capacitance gradient (*dC/dz*). Both of these parameters can be measured to sufficient accuracy, to meet the aims of the low force measuring instrument project, using existing voltage and capacitance measuring instrumentation. It is, therefore, considered unnecessary to implement the "virtual work" concept in the proposed device design for force measurements in the range 10 μN to 1 nN (Robinson and Kibble 2002). Although the virtual work concept, if implemented, appears to offer useful cross checking capability, it involves additional complications (such as velocity, current and resistance measurements), and at the level of accuracies being sought in this project the virtual work implementation is unlikely to be of any practical use. Thus, the virtual work concept implementation should only be contemplated if a few tens of parts-per-million accuracies or better in the range of micro- to nanonewton force measurements are required.

3 THE PROPOSED MODEL

Figure 8 is a schematic diagram of a practical realisation of a four-plate capacitor. The diagram shows the two sets of parallel plate capacitors and a screening arrangement that is necessary to minimise the effects of stray capacitance (Kibble and Rayner 1984).

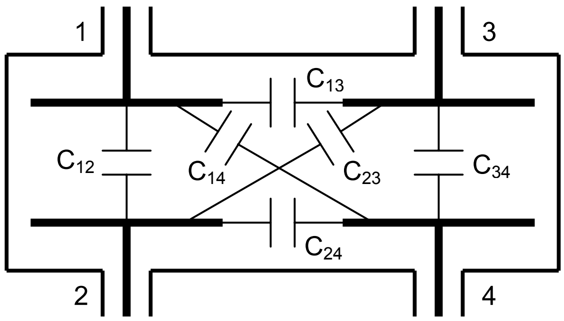

Figure 8 Schematic diagram of the proposed capacitor showing the elements of the capacitance matrix and the screening arrangement

Ignoring capacitances between the electrodes and the screen initially, there are four electrodes carrying charges Q_1 to Q_4 respectively and six independent capacitances:

$$C_{12} \quad C_{13} \quad C_{14} \quad C_{23} \quad C_{24} \quad C_{34}$$

where it is assumed by symmetry that $C_{xy} = C_{yx}$ in all cases. The four charges, by superposition, each consist of three components as given by the following equations

$$\begin{pmatrix} Q_1 \\ Q_2 \\ Q_3 \\ Q_4 \end{pmatrix} = \begin{pmatrix} C_{12}V_{12} + C_{13}V_{13} + C_{14}V_{14} \\ C_{12}V_{21} + C_{23}V_{23} + C_{24}V_{24} \\ C_{13}V_{31} + C_{23}V_{32} + C_{34}V_{34} \\ C_{14}V_{41} + C_{24}V_{42} + C_{34}V_{43} \end{pmatrix}. \tag{3.1}$$

Making the substitution, $V_{xy} = -V_{yx}$ in all cases leads to

$$\begin{pmatrix} Q_1 \\ Q_2 \\ Q_3 \\ Q_4 \end{pmatrix} = \begin{pmatrix} +C_{12}V_{12} + C_{13}V_{13} + C_{14}V_{14} \\ -C_{12}V_{12} + C_{23}V_{23} + C_{24}V_{24} \\ -C_{13}V_{13} - C_{23}V_{23} + C_{34}V_{34} \\ -C_{14}V_{14} - C_{24}V_{24} - C_{34}V_{34} \end{pmatrix}. \tag{3.2}$$

If all four rows in equation (3.2) are added together, then the relation

$$Q_1 + Q_2 + Q_3 + Q_4 = 0 \tag{3.3}$$

is obtained which shows that the total charge on the system is always zero as expected. It is sufficient, therefore, to continue the analysis with just Q_1 to Q_3. A further simplification can be made by expressing all voltages relative to port (4) in Figure 8, giving

$$\begin{pmatrix} V_{12} \\ V_{13} \\ V_{23} \end{pmatrix} = \begin{pmatrix} V_{14} - V_{24} \\ V_{14} - V_{34} \\ V_{24} - V_{34} \end{pmatrix} \tag{3.4}$$

and leading finally to a set of equations, thus

$$\begin{pmatrix} Q_1 \\ Q_2 \\ Q_3 \end{pmatrix} = \begin{pmatrix} C_{12} + C_{13} + C_{14} & -C_{12} & -C_{13} \\ -C_{12} & C_{12} + C_{23} + C_{24} & -C_{23} \\ -C_{13} & -C_{23} & C_{13} + C_{23} + C_{34} \end{pmatrix} \begin{pmatrix} V_{14} \\ V_{24} \\ V_{34} \end{pmatrix}. \tag{3.5}$$

A capacitance bridge will have an alternating source voltage and will measure the associated alternating current to determine the capacitance

$$\begin{pmatrix} i_1 \\ i_2 \\ i_3 \end{pmatrix} = \begin{pmatrix} C_{12} + C_{13} + C_{14} & -C_{12} & -C_{13} \\ -C_{12} & C_{12} + C_{23} + C_{24} & -C_{23} \\ -C_{13} & -C_{23} & C_{13} + C_{23} + C_{34} \end{pmatrix} \begin{pmatrix} j\omega v_{14} \\ j\omega v_{24} \\ j\omega v_{34} \end{pmatrix} \tag{3.6}$$

where i_1 to i_3 refers to the current measured at ports (1) to (3) respectively, ω is the angular frequency of the source, v_{ij} is the alternating voltage and j is the square root of -1. The measurements required to define the capacitance matrix given by equation (3.6) are discussed in §5.

Finally, the following equation is used to calculate the force from the capacitance matrix in, say the x direction

$$F_x = \frac{1}{2} \mathrm{V}^{\mathrm{T}} \left(\frac{d}{dx} \mathrm{C} \right) \mathrm{V} \tag{3.7}$$

where V is the second term on the right hand side of equation (3.5) and C is the capacitance matrix in equation (3.5). Note that equation (3.7) is the four-plate version of equation (2.1).

4 FINITE ELEMENT MODELLING OF THE PROPOSED DESIGN

4.1 THEORETICAL BASICS

The behaviour of the four-plate capacitor system was simulated using a finite element program called "HiPhi" from Field Precision. The aim was to estimate forces that would be applied on the dielectric blade as it is pulled out of equilibrium. The *primary force* is that along the vertical direction (which we will call x) which balances the applied force under test. However, lateral forces will also exist and these need to be estimated. Also torques may exist due to the couples set up between the four electrodes and the blade. Further, changes in the primary force if the blade is displaced away from its equilibrium position were calculated - this issue is considered to be the most important since it is hoped that lateral forces and torques can be compensated for due to the high relative stiffness of the balance in these axes. However, changes in the primary force due to unwanted displacements would lead to errors in the force calculation.

The force on the blade is given by

$$F_x = -\frac{\partial U}{\partial x}, \quad F_y = -\frac{\partial U}{\partial y}, \quad F_z = -\frac{\partial U}{\partial z}, \tag{4.1}$$

where (x, y and z) refers to the centre of mass of the blade and U is the total potential energy of the system. Note that the capacitor is connected to an external circuit consisting (say, for simplicity) of a battery. Therefore,

$$U = U_c + U_b \tag{4.2}$$

where U_c is the potential energy of the capacitor system and U_b is the potential energy of the battery (external circuit). Also torques are given by

$$\tau_x = -\frac{\partial U}{\partial \theta_x}, \quad \tau_y = -\frac{\partial U}{\partial \theta_y}, \quad \tau_z = -\frac{\partial U}{\partial \theta_z}, \tag{4.3}$$

where θ_x refers to rotation about the x axis, *etc.*

In the computer simulation the extended Poisson's equation of the following form was solved (Grant and Phillips 1984)

$$\nabla \cdot (\varepsilon \, \nabla \phi) = 0 \tag{4.4}$$

where $\varepsilon(\mathbf{r})$ is the permittivity and $\phi(\mathbf{r})$ is the electric potential. The boundary condition is a specified fixed potential on the electrodes and

$$\frac{\partial \phi}{\partial n} = 0$$

at the simulation boundaries - this attempts to approximate free space, where n is the unit normal at a boundary. Having solved equation (4.4) the potential energy of the capacitor is calculated as

$$U_c = \int_V \tfrac{1}{2}\varepsilon|\mathbf{E}|^2 \, dV \tag{4.5}$$

where the electric field is calculated from

$$\mathbf{E} = -\nabla\phi \, . \tag{4.6}$$

For force calculations the total stored energy including the battery energy, U_b, must be calculated. In particular the total energy change when the blade is moved needs to be calculated so as to calculate forces from equation (4.1). The next section describes how the change in the battery stored energy is calculated.

4.2 CALCULATION OF THE TOTAL ENERGY CHANGE DUE TO REARRANGING THE CHARGES IN A FIXED POTENTIAL FOUR-PLATE CAPACITOR

When the dielectric is moved the capacitance matrix of the system changes. Since potentials are fixed the charges on the plates must change. If the charges before the plate is moved are Q_1, …, Q_4 and the charges after a displacement are Q_1', …, Q_4' then the energy change of the capacitor system is

$$\Delta U_c = \frac{1}{2}\Delta Q_1 V_1 + \frac{1}{2}\Delta Q_2 V_2 + \frac{1}{2}\Delta Q_3 V_3 + \frac{1}{2}\Delta Q_4 V_4 \tag{4.7}$$

where $\Delta Q_1 = Q_1' - Q_1$, *etc.*

However, in order for the charges on the plates to change they must flow *through the external circuit* and when this happens the battery does work on the charges. Thus the total energy change is the change in the energy of the capacitor plus the work done by the battery. To calculate the work done by the battery we imagine the charge flowing between the fixed potentials. There are several ways to go from the initial to final configuration of charges but the work done should not depend on the route. Figure 9 shows an example route and the amount of work done to rearrange the charges at each stage. The total work done is (from Figure 9)

$$\begin{aligned} W_{tot} &= (V_1 - V_3)(Q_1' - Q_1) + (V_2 - V_4)(Q_2' - Q_2) + (V_3 - V_4)(Q_3' - Q_3 - Q_1 + Q_1') \\ &= V_1\Delta Q_1 + V_2\Delta Q_2 + V_3\Delta Q_3 + V_4\Delta Q_4 \end{aligned} \tag{4.8}$$

where we have used

$$Q_1 + Q_2 + Q_3 + Q_4 = Q_1' + Q_2' + Q_3' + Q_4'$$

so that

$$\Delta Q_1 + \Delta Q_2 + \Delta Q_3 + \Delta Q_4 = 0 .$$

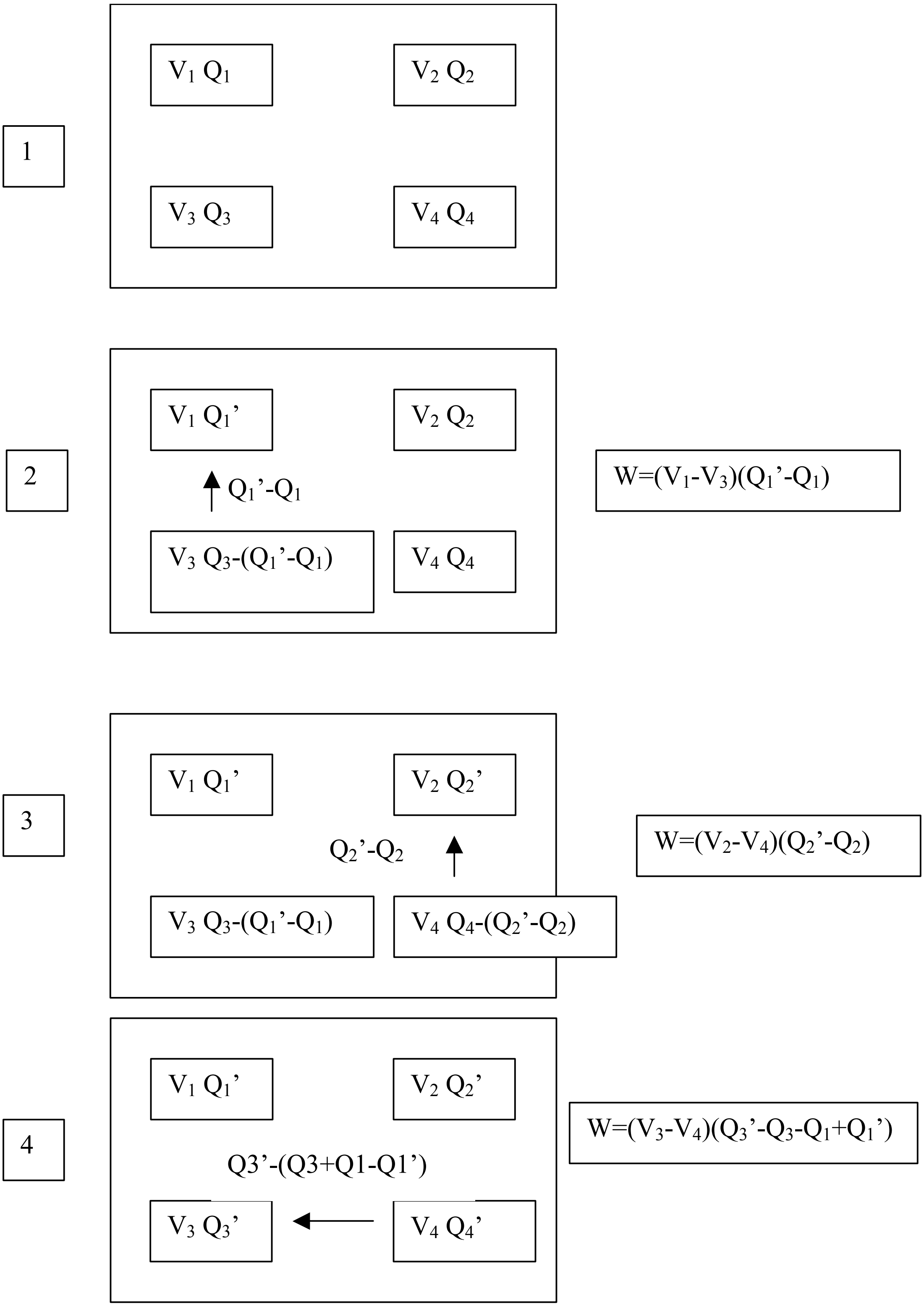

Figure 9 Transferring charge between the plates from initial to final (primed) configuration. Work done at each step is shown. The final charge on plate 4 after stage (4) is Q_4' owing to conservation of charge: $Q_1 + Q_2 + Q_3 + Q_4 = Q_1' + Q_2' + Q_3' + Q_4'$

The energy change of the battery is, therefore, given by

$$\Delta U_b = -W_{tot} = -(V_1\Delta Q_1 + V_2\Delta Q_2 + V_3\Delta Q_3 + V_4\Delta Q_4) = -2\Delta U_c \,. \qquad (4.9)$$

Hence

$$\Delta U_{tot} = \Delta U_c + \Delta U_b = -\Delta U_c \,. \qquad (4.10)$$

So we can calculate the total energy change as the negative of the capacitor energy change.

4.3 COMPUTER SIMULATION

Figure 10 shows the computer simulation geometry of the proposed design of four-plate capacitor. In simulation the four electrodes are taken to be infinitely thin and made of perfect metal with fixed potential. The dielectric blade and dielectric backing (top and bottom) are made of fused silica ($\varepsilon_r = 3.8$). Remaining areas are treated as vacuum. Note that the simulation is carried out in three dimensions with a suitably large distance between the geometry regions and the simulation boundaries.

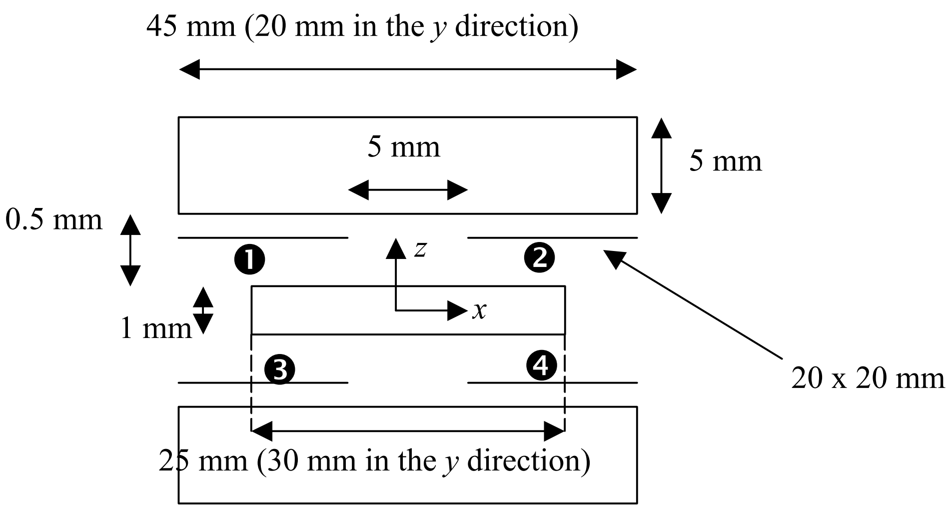

Figure 10 Computer simulation geometry. The dielectric blade is in the middle and the top and bottom rectangles are the dielectric backing

Figure 11, Figure 12 and Figure 13 show the simulation meshing for the unperturbed configuration (blade at the central position and not rotated). The finite element model uses hexahedral elements (squashed cuboids). About 800 000 nodes are used in the simulation which takes about 7 minutes to complete on a Pentium 4, 2.4 GHz PC.

In all simulations we keep the plate potentials as follows:

$V_1 = 0$ V, $V_2 = 100$ V, $V_3 = 90$ V, $V_4 = 90$ V.

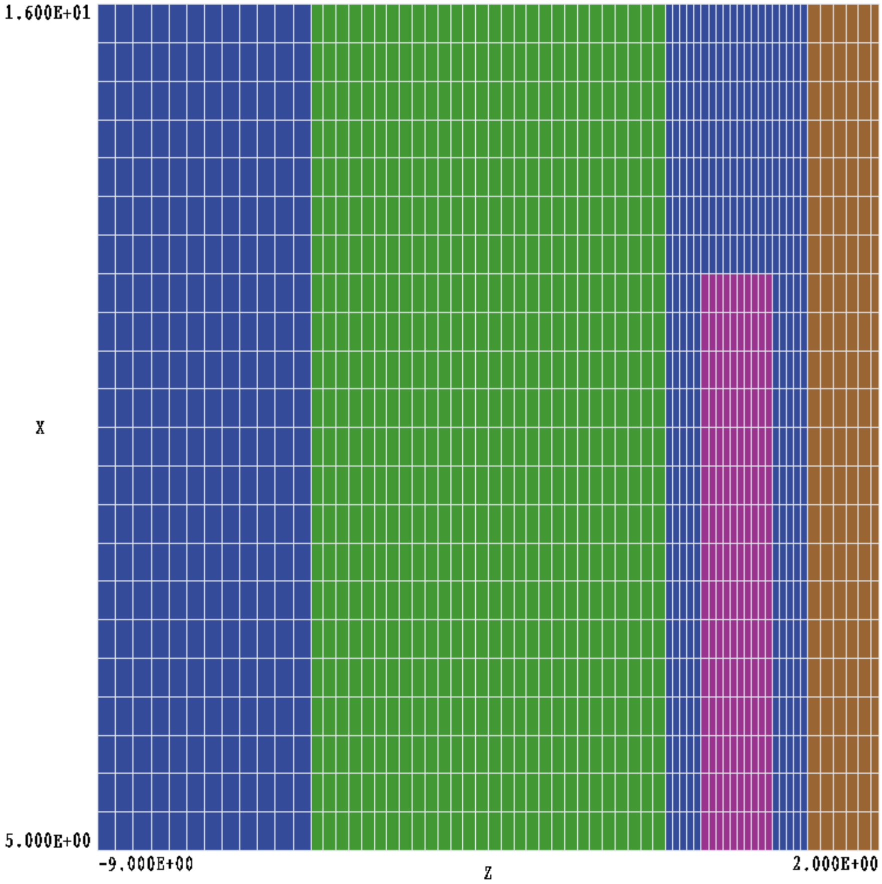

Figure 11 *y* cut (close up) showing dielectric blade (pink) between dielectric backing (green and brown). Note that variable meshing is used

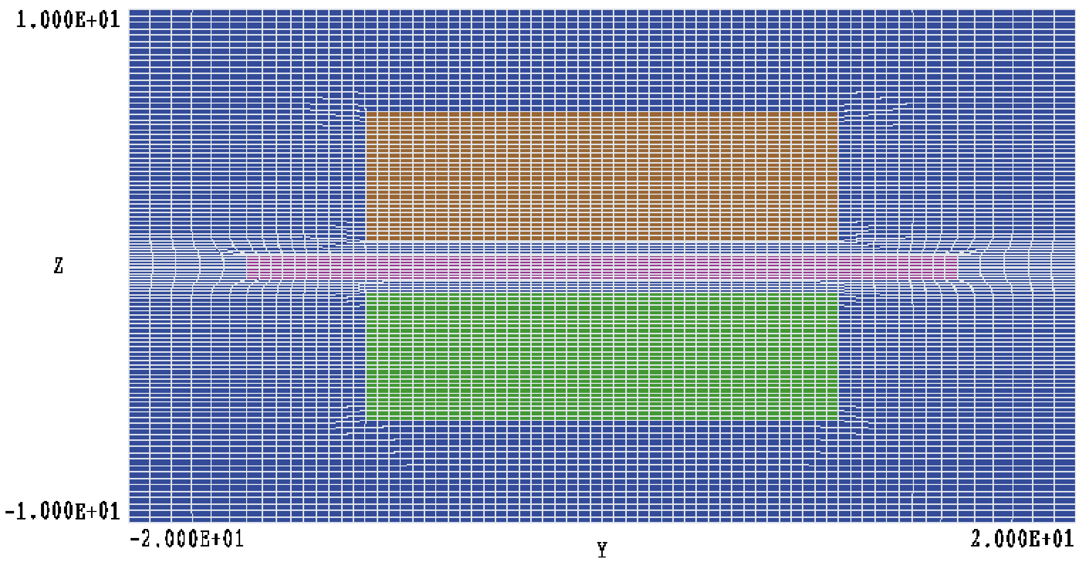

Figure 12 *x* cut showing blade between dielectric backing. Full simulation area is shown

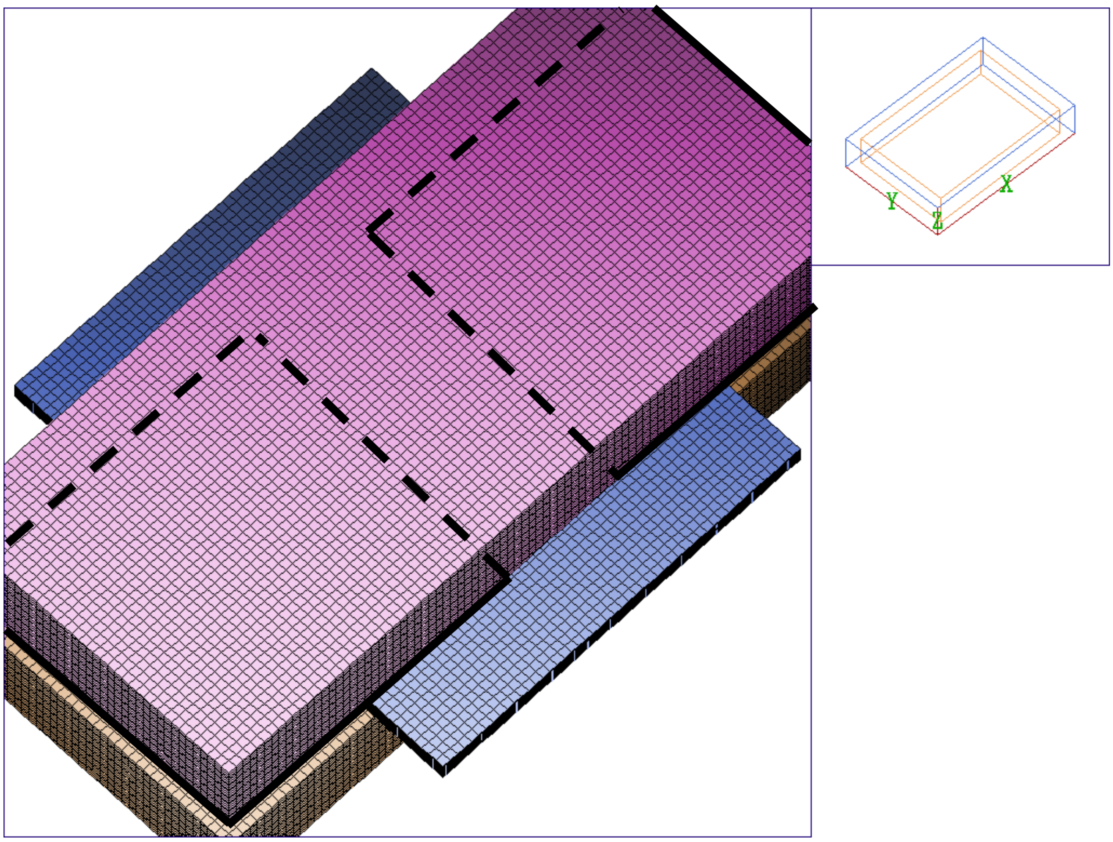

Figure 13 3D picture of capacitor modelling showing meshing. The top electrodes (1 and 2) are shown dashed

4.4 UNPERTURBED SIMULATION RESULTS

Figure 14, Figure 15 and Figure 16 show the results of the unperturbed simulation. Figure 14 shows potential contour lines in a *y*-cut. Note that the field magnitude (density of contour lines) is lower inside the dielectric blade. Most electric field goes from plate (3) to plate (1) but there is also considerable coupling between plates (1) and (2). Figure 15 shows the actual electric field magnitude and direction confirming these observations. Figure 16 shows the equipotential surface $\phi = 50$ V.

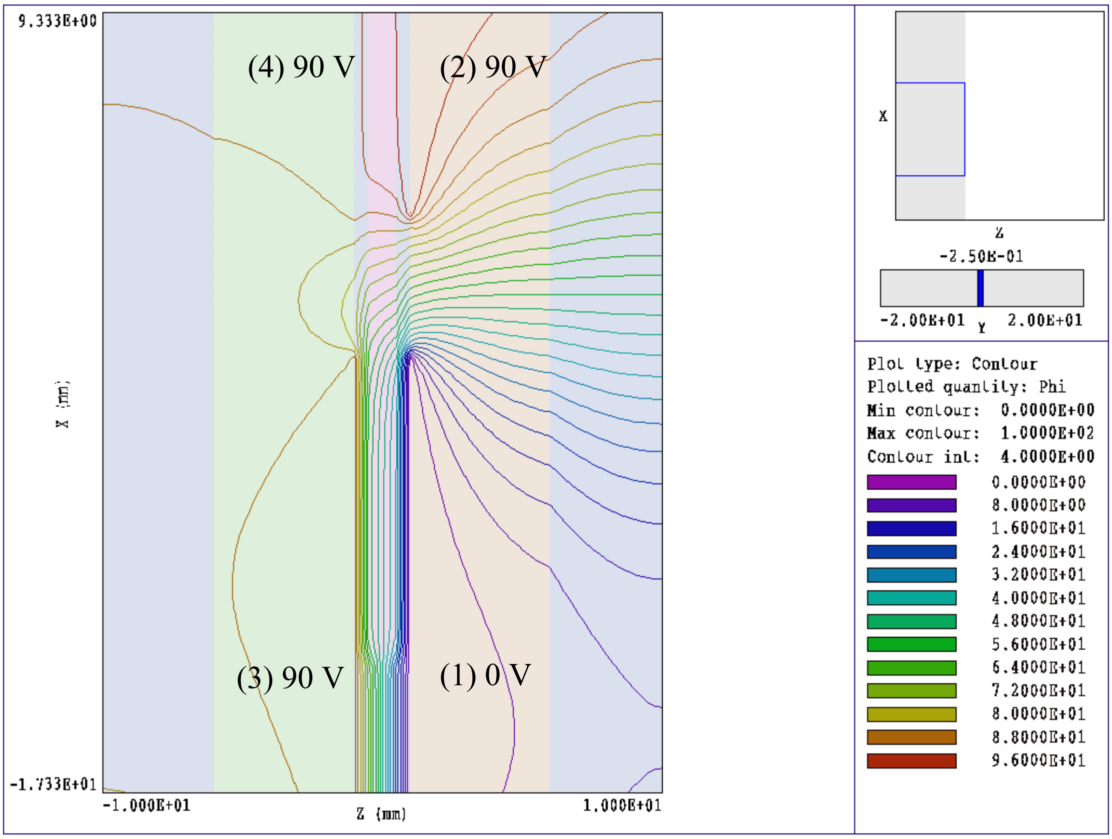

Figure 14 ϕ contour lines in unperturbed simulation (y cut). The plate numbers and potentials are shown

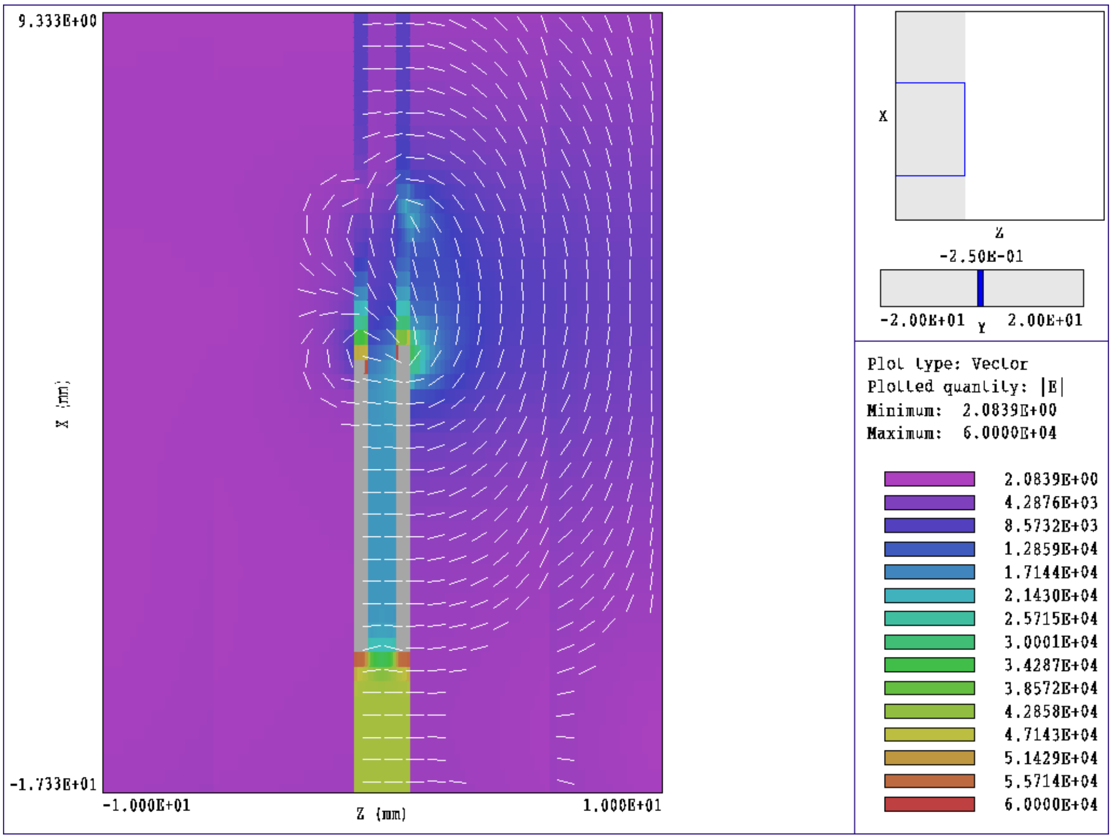

Figure 15 Electric field lines and field strength. Note that fields greater than 6 x 10^4 V m^{-1} are shown in grey

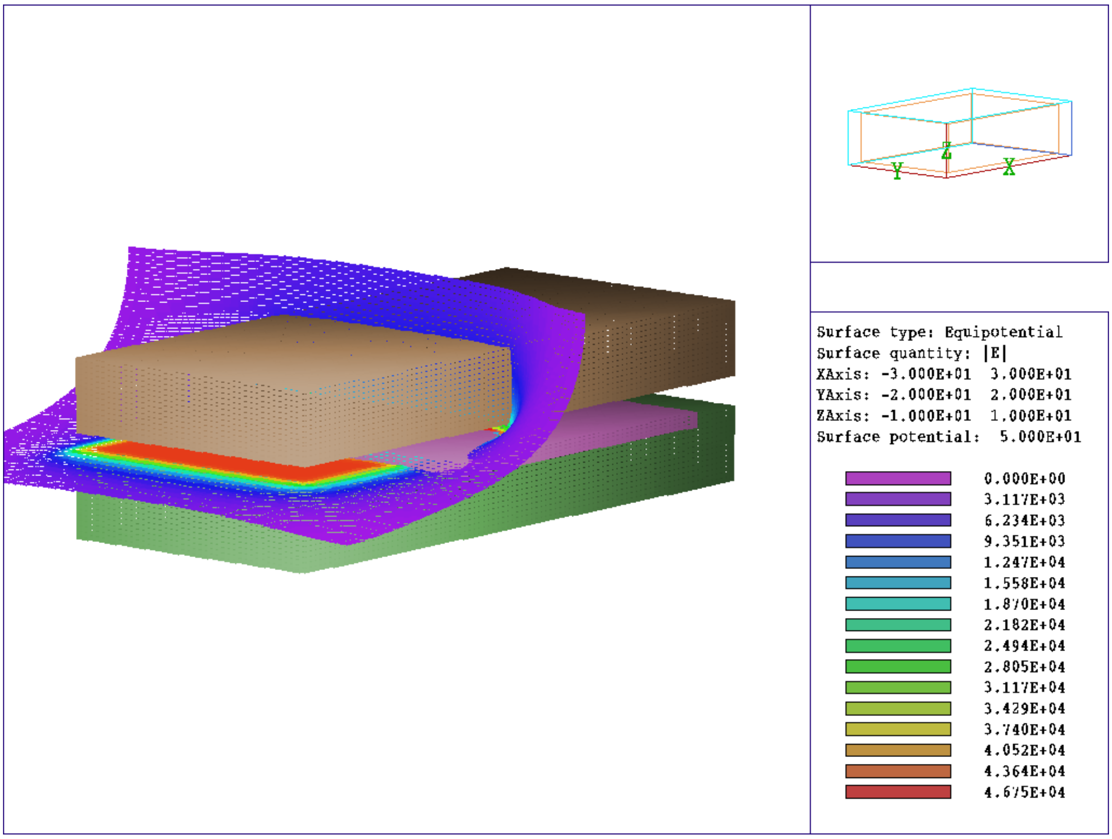

Figure 16 Equipotential surface at $\phi = 50$ V. The electric field magnitude is painted on the surfaces showing strong fields between plates (1) and (3): 0 V and 90 V

4.5 PRIMARY FORCE SUSCEPTIBILITY TO LATERAL SHIFTS AND ROTATIONS

We now perturb the blade and recalculate energy so as to derive forces from equation (4.1). In this section we first shift or rotate the blade and then move it along the x-direction so as to calculate F_x. The aim is to discover how much the primary force, F_x, is altered by lateral shifts and rotations. Figure 17 shows energy change as we shift along x direction with the blade displaced by z = 0, 0.1 mm, 0.2 mm and 0.3 mm. Note that the energy variation with x is linear indicating F_x is approximately constant. Also the gradient of each curve is approximately the same showing that F_x is only weakly affected by z-shifts. Note, however, that the absolute amount of energy is altered by the z-shift. These plots are actually capacitor energy, U_c, whereas the total energy is $-U_c$, therefore, we see that the system loses energy when the blade moves along z closer to the electrodes. So the blade will be pulled towards the electrodes (as will also be shown in the next section). Figure 18 shows the actual forces as indicated by differentiating energies in Figure 17. The force is approximately constant when the blade is moved along x and the variation of force with z-shift is relatively small. A z-shift of 0.3 mm from the symmetric configuration causes a primary force change of 16 nN (2%). Note that the blade is pulled along the $-x$ direction, it wants to be between plates (1) and (3), with potential difference is 90 V since that way it can minimise the energy of the system.

Figure 19 and Figure 20 similarly show the effect of *y*-shifts. There is very little effect here because shifting along *y* does not move the blade closer to the electrodes. A *y*-shift as high as 3 mm only alters the primary force by 1.2 nN.

Figure 21, Figure 22 and Figure 23 show the effect of rotations on primary force. We see that *y*-rotations (Figure 22) have the most effect because this swings the long end of the blade towards the electrodes. It seems to be essential to keep rotations less than 0.4º. Figure 24 shows the blade at 1.6º *y*-rotation, indicating that the ends are then very close to the electrodes. The *z*-rotation has almost no effect (Figure 23).

Note that these graphs take a lot of computer power to produce. For example, Figure 17 takes twenty separate runs at 7 minutes each giving a total computation time of 2.3 hours.

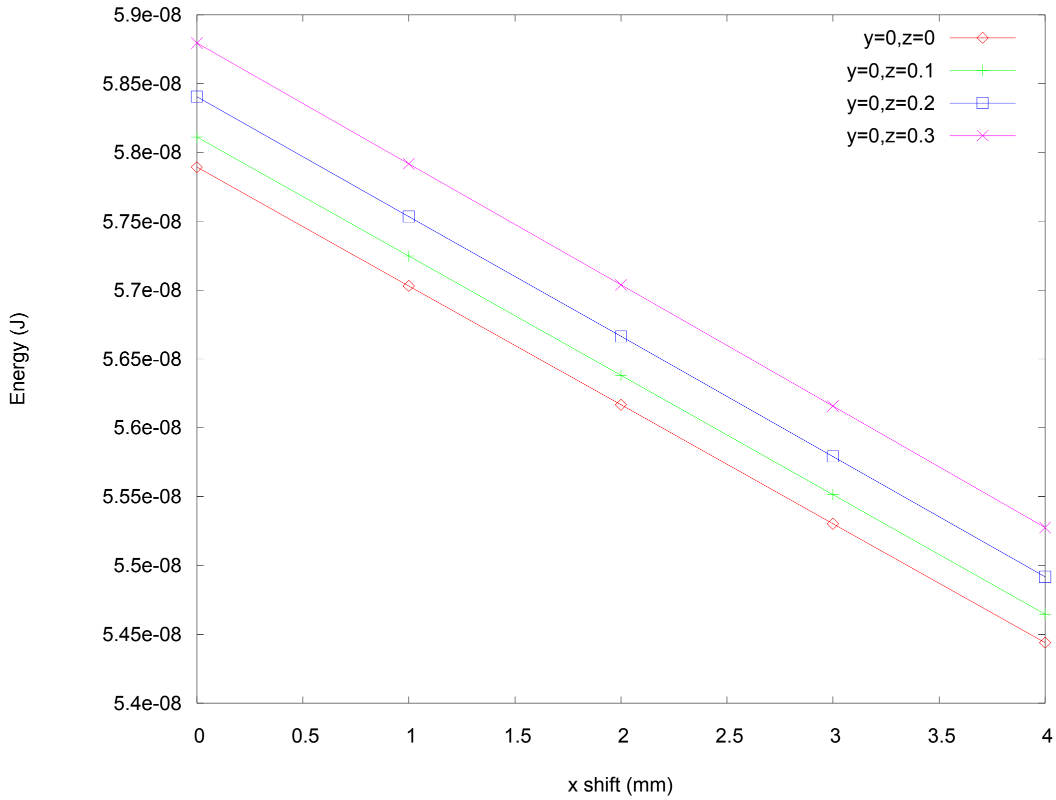

Figure 17 Change in energy when blade is shifted along *z* direction (in mm) and then along *x* (primary) direction

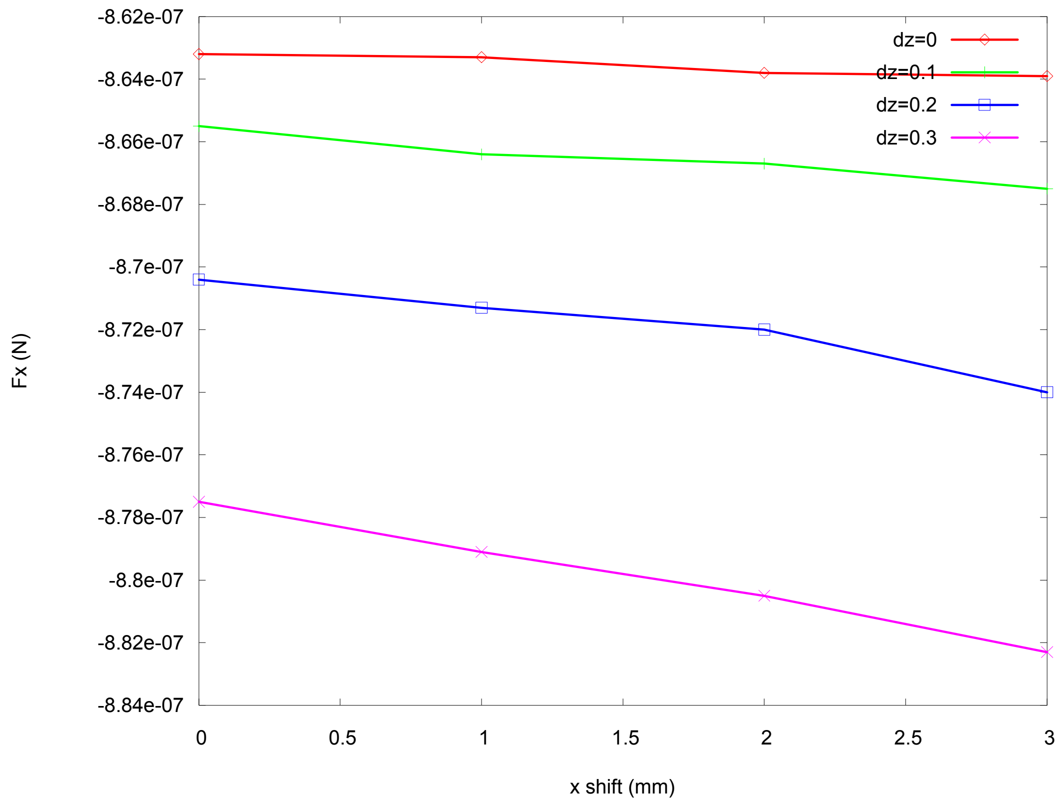

Figure 18 Force variation with *z* shift from derivative of Figure 17

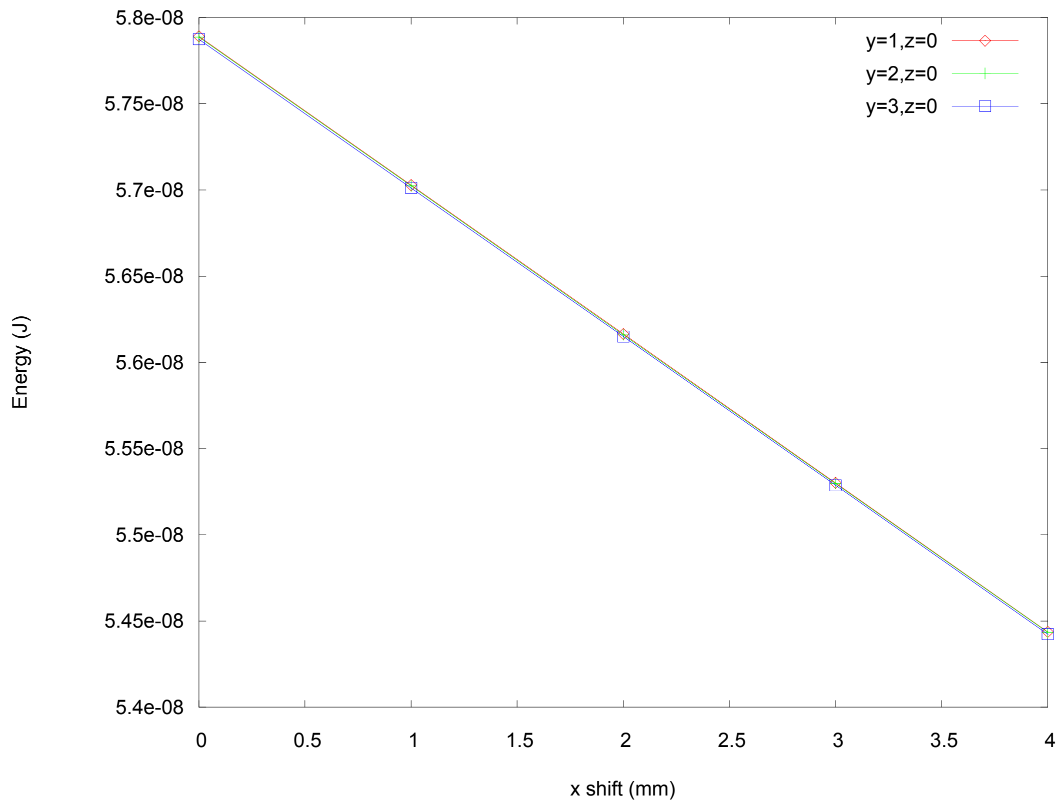

Figure 19 Energy change as blade is shifted along *y* (mm) and then along *x*

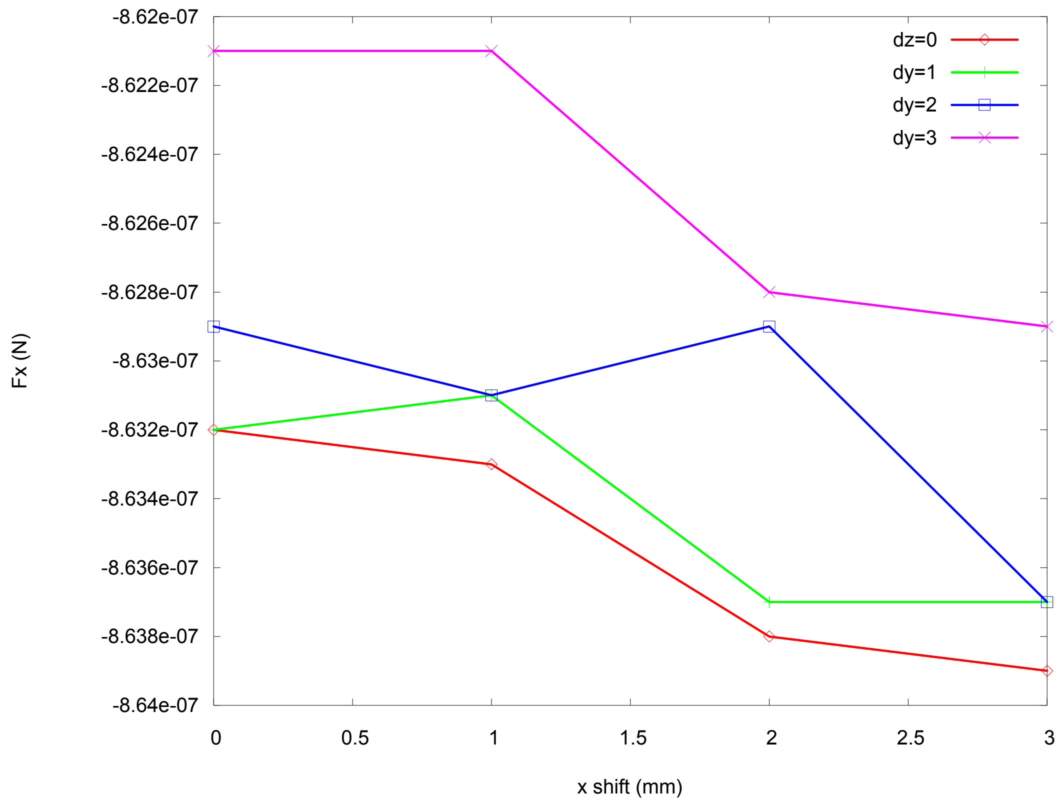

Figure 20 Force variation from *y* shift from derivative of Figure 19

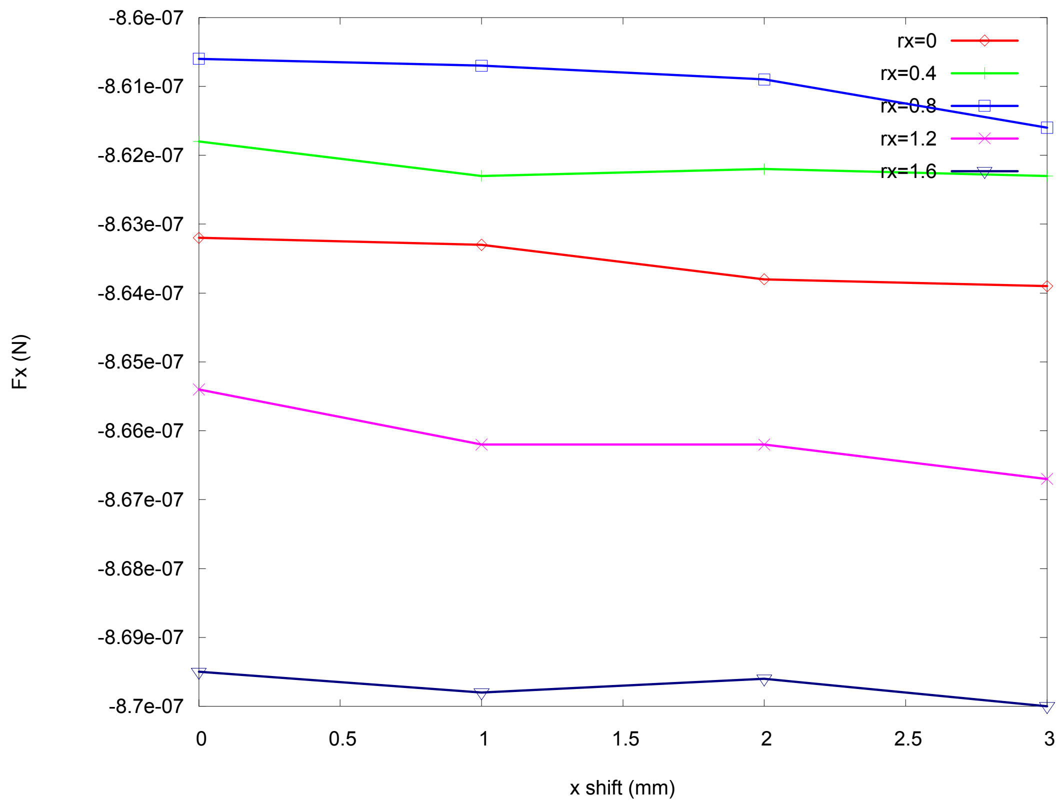

Figure 21 Primary force variation for different *x* rotations (in degrees)

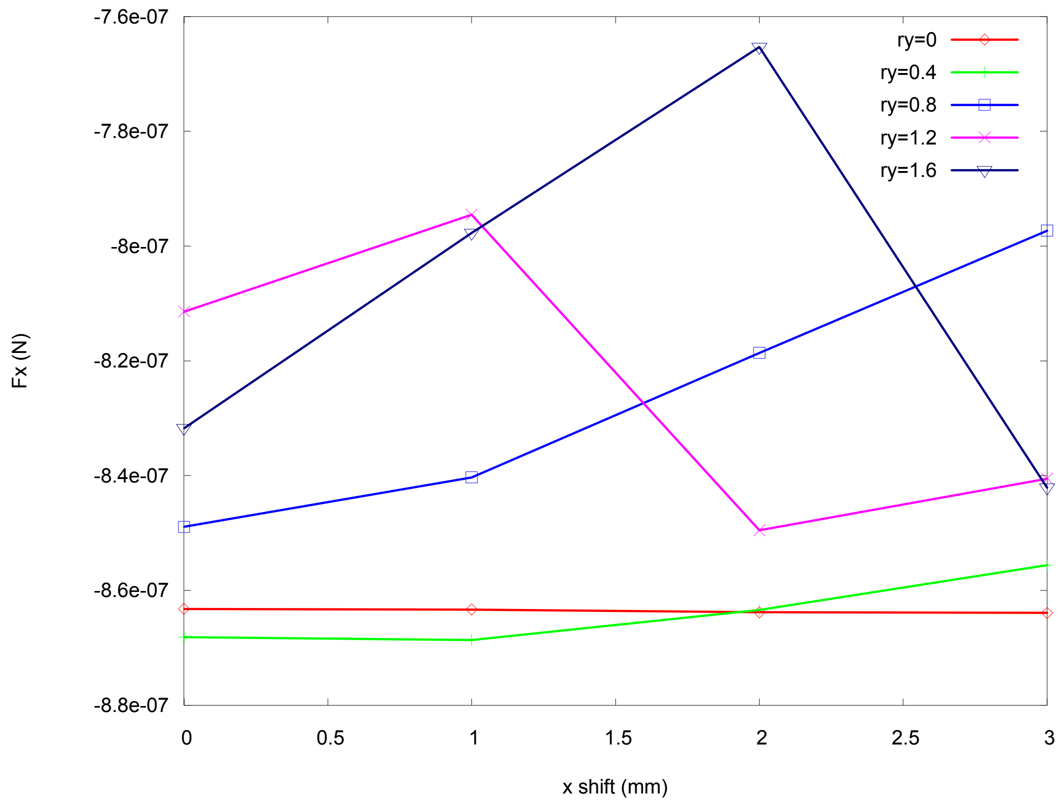

Figure 22 Primary force variation for different *y* rotations (in degrees)

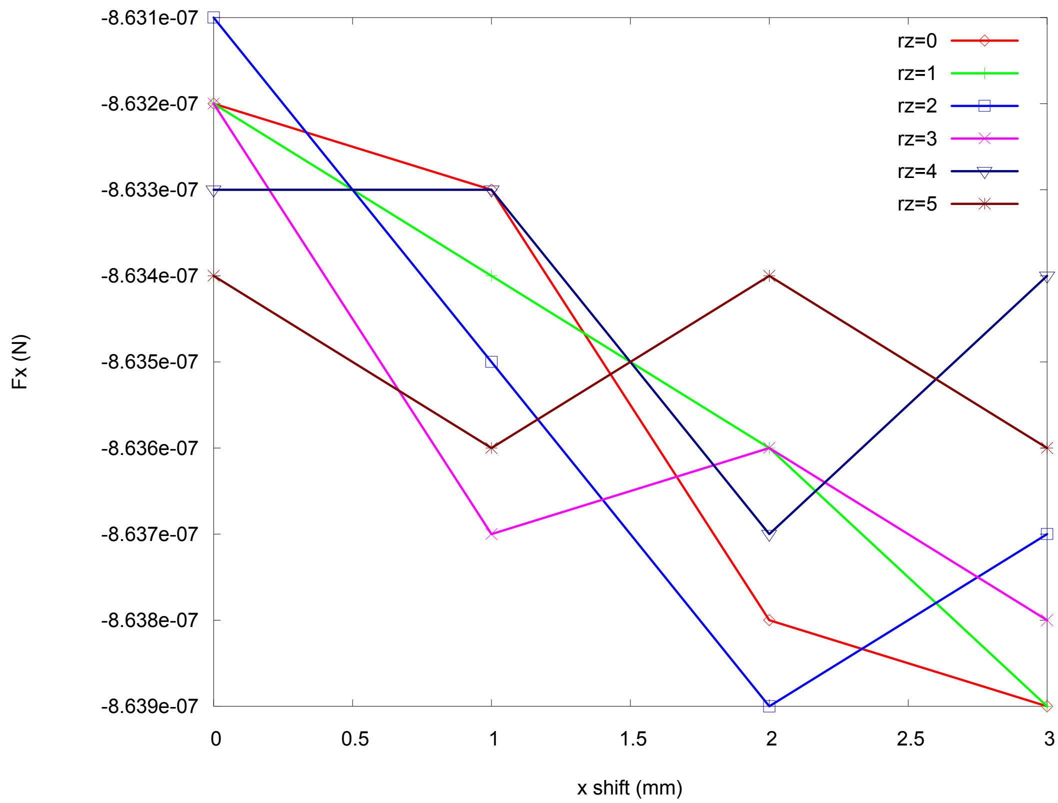

Figure 23 Primary force variation for different *z* rotations (in degrees)

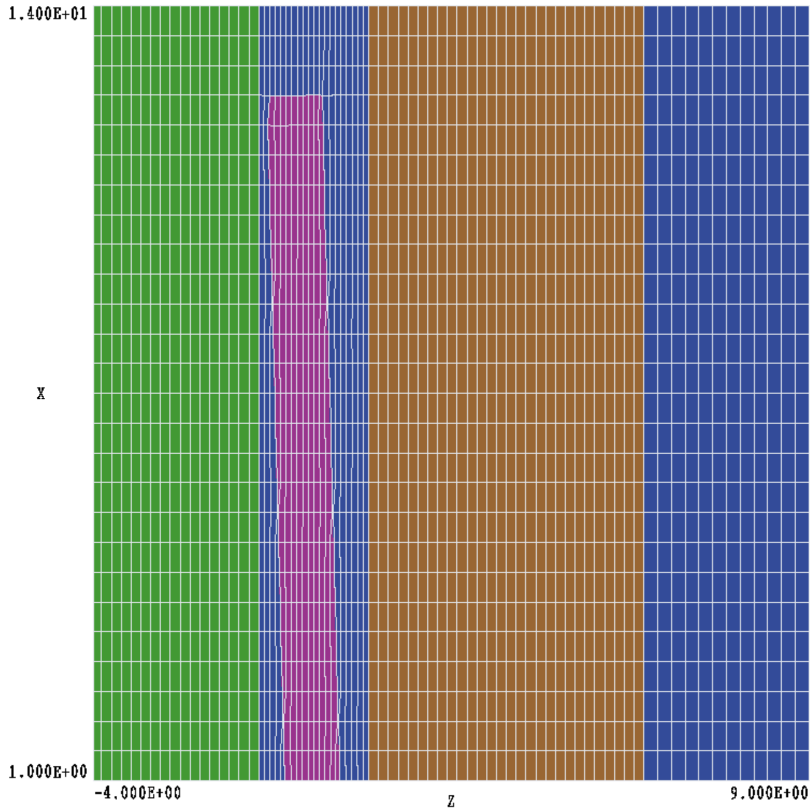

Figure 24 Blade rotated about *y* through 1.6°

4.6 LATERAL FORCES

The lateral forces on the blade were then estimated. These will need to be compensated for in the balance. We move the blade along the *y*- and *z*-directions and calculate F_y and F_z from equation (4.1). Also, we rotate the blade along the primary axis and calculate torque from equation (4.2).

Figure 25 shows $F_y(y)$. As anticipated the forces are very low, about a two hundred times lower than the primary force, F_x, shown above. By contrast, Figure 26 shows that the lateral force F_z is about five times *higher* than the primary force indicating that the blade is strongly pulled towards electrodes (1) and (2) which have a 100 V potential difference. Figure 27 shows the *x*, *y* and *z* torques as the blade is rotated about corresponding axes. As anticipated the *z* torque is very low and the *y*-torque is highest. The "W" shape of the *y*-torque is because of the finite meshing in the system; an average value should be taken of these points.

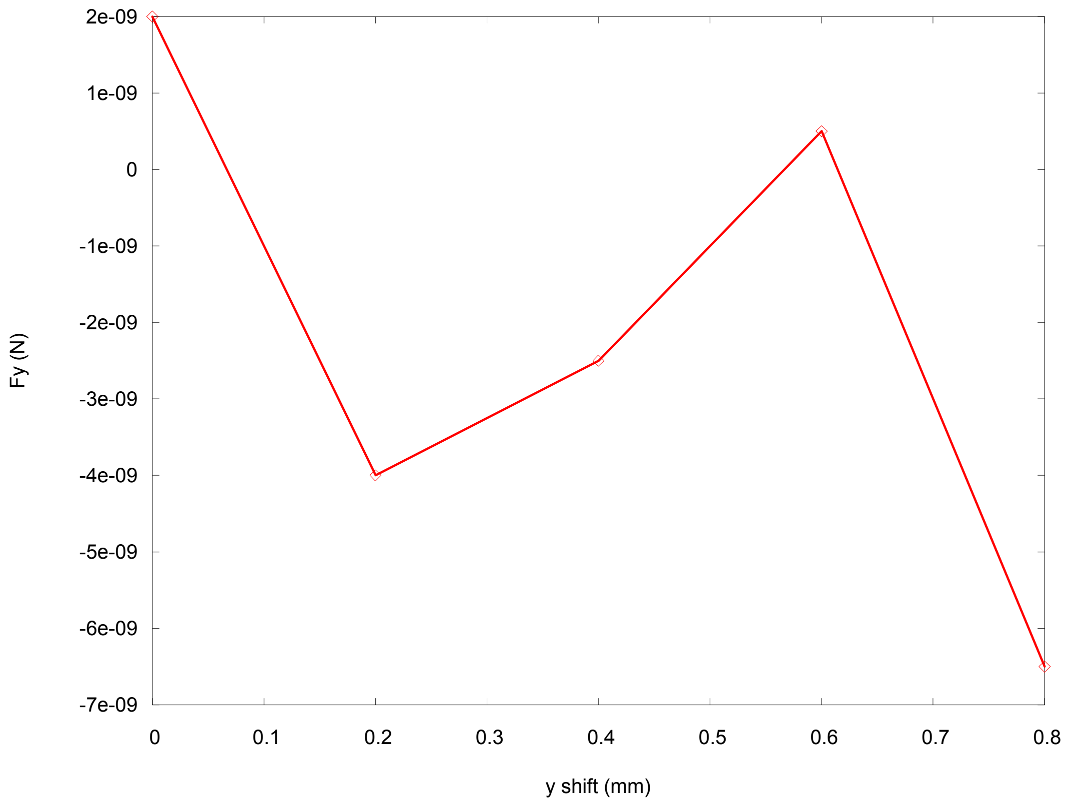

Figure 25 Graph of lateral force $F_y(y)$

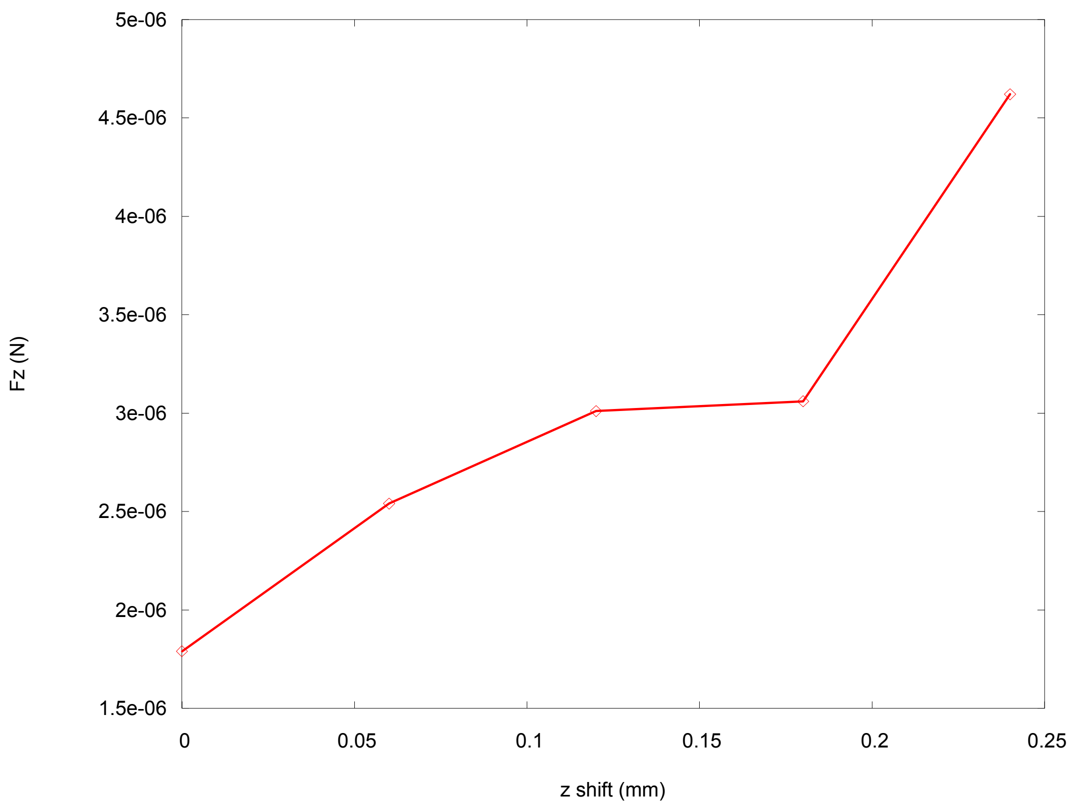

Figure 26 Graph of lateral force $F_z(z)$

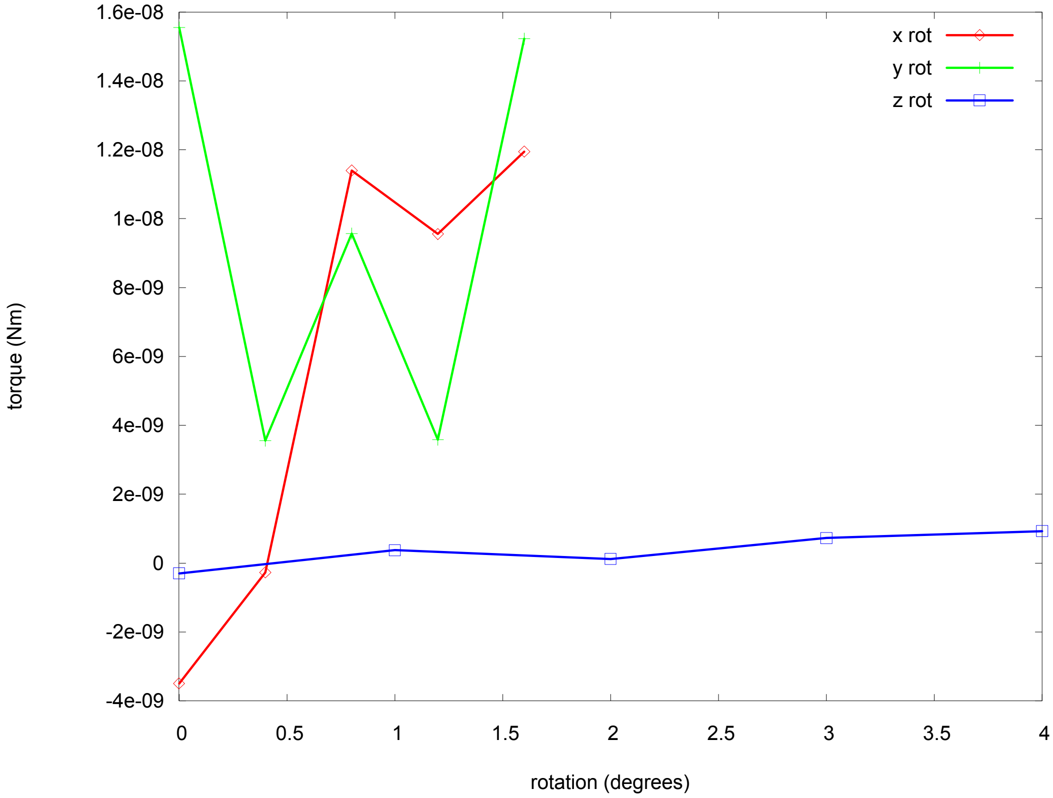

Figure 27 Graph of torque variation: $\tau_x(\theta_x)$, $\tau_y(\theta_y)$ and $\tau_z(\theta_z)$

4.7 ADDITIONAL OBSERVATIONS

Some additional computer simulations were carried out with the following results:

1. Potentials V_1= 0 V, V_2= 100 V, V_3= V_0 V, V_4= V_0 V with V_0 varied between 90 V and 50 V. The results are basically the same but decreasing V_0 decreases the primary force since this is mainly due to the blade trying to move between plates (1) and (3) rather than between (2) and (4) due to the difference between V_{13} and V_{24}. For V_0 = 50 V, these two potential differences are the same so there is no primary force.

2. An alternative "zigzag" potential scheme V_1= V_0 V, V_2= 100 V, V_3= 0 V, V_4= V_0 V was modelled (see Figure 10). However, this did not significantly alter lateral forces or torques.

4.8 NOTES ON NUMERICAL ACCURACY OF THE SIMULATIONS

To check the simulation is finely enough meshed and has enough "air" volume, the simulation was repeated with more mesh points. The "big" simulation has 900,000 mesh points, corresponding to the simulations of section 4.4, compared to a "small" simulation with 500,000 mesh points. The simulation volume is larger for the big simulation (*i.e.* distance from structure to boundaries is greater). The simulation run times scale approximately linearly with mesh points.

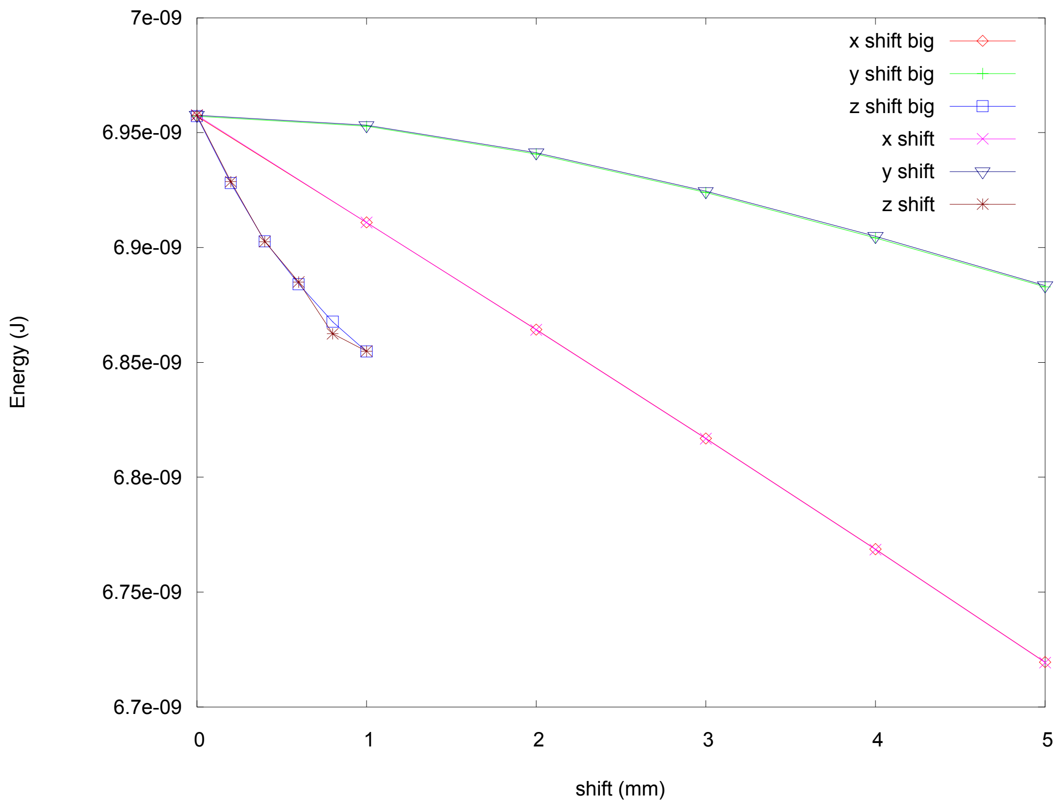

Figure 28 Energy due to shifting the dielectric blade for a big and small simulation. The small simulation energy has been shifted upwards by 0.55 x 10^{-9} J to make the graphs coincide

Figure 28 shows energy curves for the two simulations (note these simulations where for a slightly different geometry than shown in figure 10; the electrodes were volumetric rather than flat). The graphs agree but only when the energy is shifted by 0.55×10^{-9} J (the big simulation has more stored energy). It seems that the boundaries store some energy that depends on the closeness of the boundary. However, this energy is not affected by blade shifts and so has no effect on forces or torques that depend on derivatives. This tendency for boundaries to store constant energy – and so renormalise the energy zero – is common in capacitor calculations. If absolute values of capacitance are measured it is normally necessary to calibrate the simulation using experimental data.

5 MEASUREMENT OF THE CAPACITANCE MATRIX

Measurements of the six capacitances are illustrated in the Table 1 below. Note that the voltages at all ports *must be defined by a low impedance.* This is either done with a short circuit or with the bridge connections as shown in Figure 29. The bridge drives the source voltage, represented by the oscillator symbol, with a low impedance and maintains zero voltage at the detector port, represented by the ammeter symbol, with a low impedance whilst measuring the current flowing. The return current path is *via* the overall screen surrounding the bridge and the capacitor system. Only the current flowing at port (1) in this illustration contributes to the measurement; the current flowing in the short circuits at ports (2) and (3) return to the oscillator without being measured. In Table 1, this figure is shown in abbreviated form with 'S' representing the bridge source and 'D' representing the bridge detector.

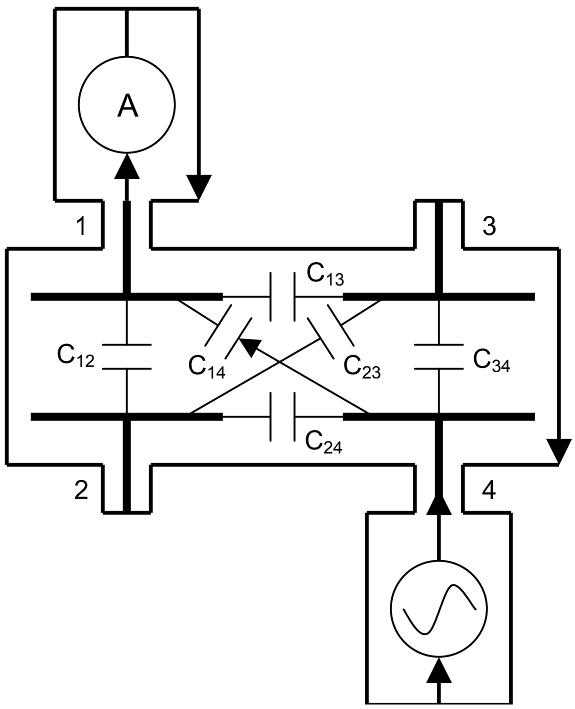

Figure 29 Capacitance bridge connection scheme showing the function of the source, detector and screen together with

Configuration	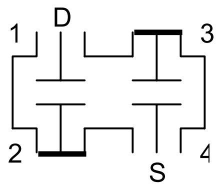	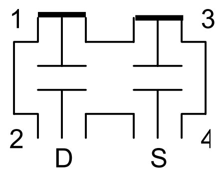	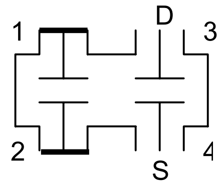
$\begin{pmatrix} V_{14} \\ V_{24} \\ V_{34} \end{pmatrix}$	$\begin{pmatrix} 1 \\ 1 \\ 1 \end{pmatrix}$	$\begin{pmatrix} 1 \\ 1 \\ 1 \end{pmatrix}$	$\begin{pmatrix} 1 \\ 1 \\ 1 \end{pmatrix}$
Current	i_1	i_2	i_3
Source	4	4	4
Detector	1	2	3
Capacitance	C_{14}	C_{24}	C_{34}

Configuration	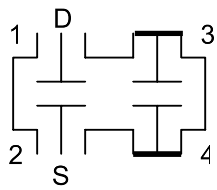	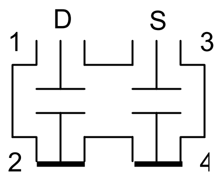	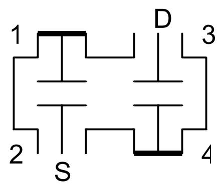
$\begin{pmatrix} V_{14} \\ V_{24} \\ V_{34} \end{pmatrix}$	$\begin{pmatrix} 0 \\ 1 \\ 0 \end{pmatrix}$	$\begin{pmatrix} 0 \\ 0 \\ 1 \end{pmatrix}$	$\begin{pmatrix} 0 \\ 1 \\ 0 \end{pmatrix}$
Current	i_1	i_1	i_3
Source	2	3	2
Detector	1	1	3
Capacitance	C_{12}	C_{13}	C_{23}

Table 1 Measurements required to fully realise all six capacitances where S refers to the bridge source and D refers to the bridge detector

During all the necessary measurements, capacitances between the electrodes and the screen have been eliminated as current flowing through them returns *via* the screen to the source without being measured. However, these capacitances may also have field lines that pass through the dielectric element and, therefore, may also contribute to the force. They, therefore, need to be measured by making use of a second screen as shown in Figure 30.

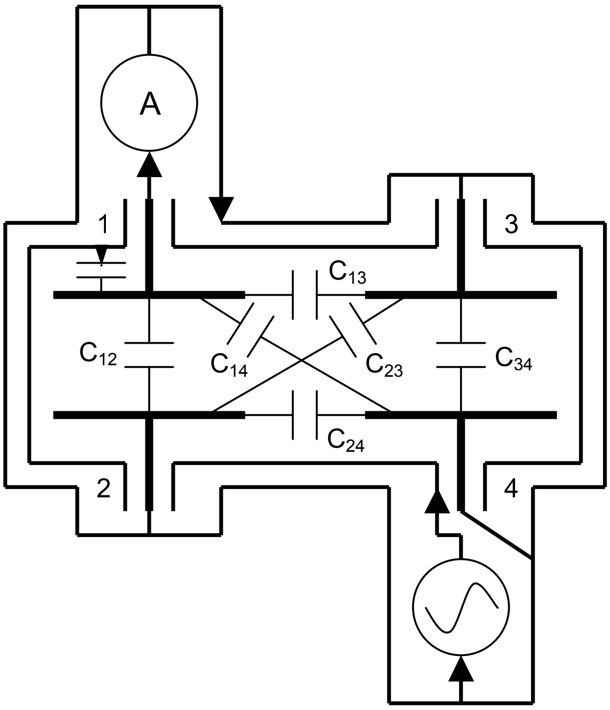

Figure 30 Introduction of an extra outer screen to enable the capacitance between the electrodes and the original (inner) screen to be measured

Each output port is now fitted with a triaxial connector that has to be interfaced to the coaxial connector of the capacitance bridge depending on the measurement being performed.

In Figure 30, the capacitance between electrode (1) and the inner screen is being measured. The bridge detector is connected between the inner and outer conductors. The bridge source is connected between the middle and outer conductors at port (4) although any of the remaining ports can be used. It is important that the other three electrodes are connected to the outer screen as shown in Figure 9 so that they do not contribute to the capacitance measurement. The remaining capacitances for electrodes (2), (3) and (4) are measured in the same way by permuting the connections appropriately.

When making the inter-electrode capacitance measurements with the double screen, care must be taken that the two screens are correctly used. Either the inner screen can be used and the outer one not connected, or both screens must be connected together to form a single screen for the capacitance bridge. Using the outer screen with the inner screen floating will not produce the correct result.

6 PRACTICAL DESIGN ISSUES

An overall schematic of the four-plate capacitor is shown in Figure 7, Figure 10 shows its approximate dimensions and Figure 31 is a general assembly drawing (the force to be measured would be applied to the pillar at the top of the drawing). The main components are the two flat rectangular plates with conducting films deposited on them and a moving dielectric paddle. The flat plates will be manufactured from low expansion material with conducting films (for example, gold or aluminium). The flat plates will be polished and lapped to a flatness of at least $\lambda/10$ and will have a surface roughness, *Ra*, of around 1 nm. The surface roughness is the most important parameter because any surface irregularities will affect the potential differences between the plates as the dielectric plate is moved – this in turn will affect the capacitance matrix and ultimately the force measurement. The flat plates will be separated using a cut down ceramic gauge block.

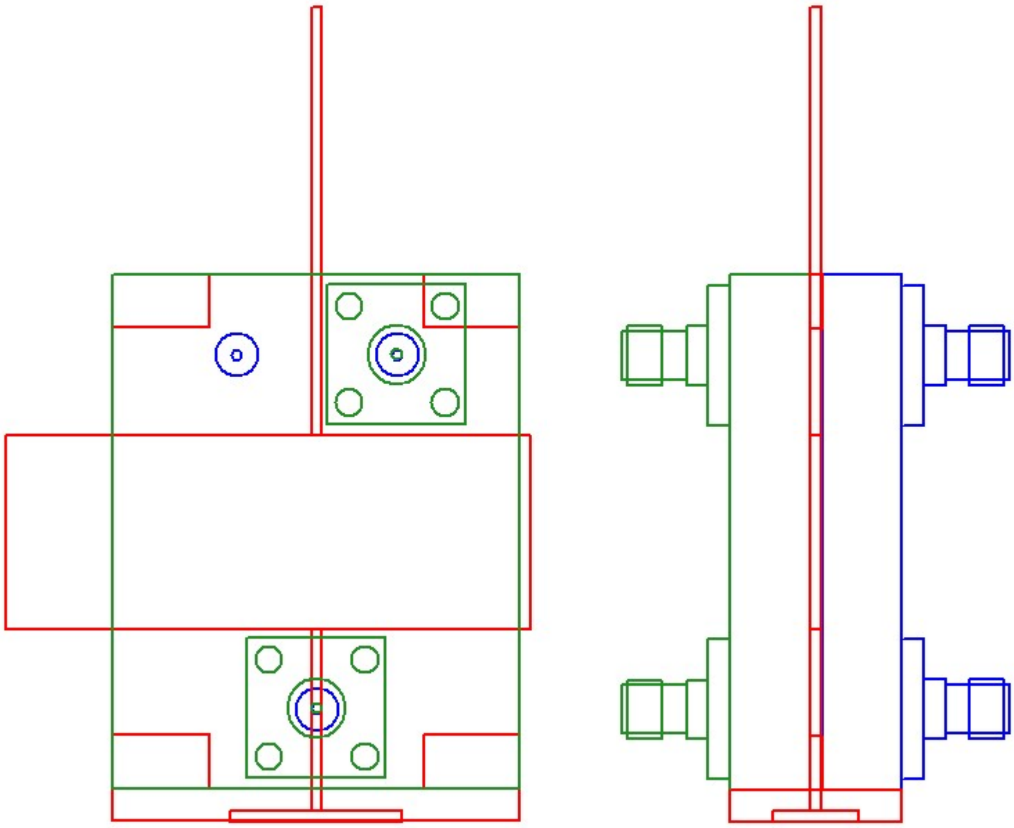

Figure 31 General assembly drawing of the capacitor

Electrical contact will be made to the conducting films by affixing a modified co-axial connector (for example, SMA) onto one side of the low expansion plate with epoxy, with the centre contact extending through the hole in the plate - but not quite flush with the opposite side. The opposite side of the hole is then filled flush with the surface with conductive epoxy (which, therefore, contacts the centre pin of the co-axial connector). The two sides of the silica plate are then vacuum coated with aluminium (with a 'bung' fitted to the open end of the co-axial connector). This aluminium, therefore, is in electrical contact with the outer of the co-axial connector (since it overcoats it) for one side, and the opposite side, the aluminium is in contact with the conductive epoxy, which is, in turn, in contact with the centre contact of the co-axial connector.

The dielectric paddle will be made from fused silica and will have the same form and surface specifications as the low expansion plates. Fused silica was chosen for its mechanical and dielectric properties. It has a relatively low thermal expansion (≈ 1 ppm K^{-1}) and has low temperature (≈ 13 ppm K^{-1}) and humidity (≈ 10 ppm per 1% change in relative humidity) coefficients of capacitance (Ford 1948, Kaplan 2003) Fused silica is also relatively easy to machine to the required tolerances and is used extensively in standard capacitors.

The double screen shown in Figure 29 will be made from double-sided circuit board that is coated in copper (this material is readily available). This will also mechanically protect the capacitor.

To measure the elements of the capacitance matrix it will be necessary make connections as per Table 1 to the capacitance bridge. It will be easier to use simple hand connections (the matrix only needs to be determined for the dC/dz determination) than to produce a complicated switch box. The bridge that will be used is a single frequency (1 kHz) Andeen-Hagerling bridge with a resolution of 0.5 aF and an accuracy of 5 ppm (model number AH2550A).

7 SUMMARY

This report has described work towards the design of a bi-directional electrostatic actuator to be used in a low force measuring instrument. The electrostatic actuator will be used to null the force being measured by applying a voltage across two sets of parallel plate capacitors with a moving dielectric. As this is a new design of actuator (in the authors' knowledge) a full theoretical analysis was required. A mathematical model of the system was set up and showed that it is necessary to measure six capacitance values in order to fully characterise the system, *i.e.* to determine the capacitance matrix. Finite element models were then used to investigate the effects of parasitic displacements and torques on the dielectric blade as the force to be measured is being applied or due to environmental effects. The models show that these parasitic effects are either negligible or that the stiffness in the axes other than the motion axis of the instrument is high enough to stop such effects having an influence on the measurement. The report then describes the practicalities of manufacturing and setting up such an actuator including the need for electrostatic screening. The system will now be manufactured and tested with the rest of the low force measuring instrument.

8 ACKNOWLEDGEMENTS

The authors wish to thank Dr Graham Hill (consultant) for help with the report and to David Flack (NPL) for reviewing the technical contents. The work was funded by the National Measurement System Policy Unit Programme for Length 2002 - 2005 Project 4.5.

9 REFERENCES

Cumpson P J, Hedley J, Zhdan P 2003 Accurate force measurement in the atomic force microscope: a microfabricated array of reference springs for easy cantilever calibration *Nanotechnology* **14** 918-924

Cumpson P J, Hedley J 2003 Accurate analytical measurements in the atomic force microscope: a microfabricated spring constant standard potentially traceable to the SI *Nanotechnology* **14** 1279-1288

Ford L H 1948 The effect of humidity on the calibration of precision air capacitors *J. IEE* **95** 13-16

Grant I S, Phillips W R 1984 *Electromagnetism* (John Wiley & Sons Ltd)

Henselmans R, Rosielle N, Cacace L, Koppelhof P, Klinkhamer F, Spierdijk H 2004 Low force measurement facility: design review report TNO/TUE Report

Hughes E B, Oldfield S 2002 Traceable, high accuracy thrust measurement for electric propulsion *28th Int. Electric Propulsion Conf., 17 – 21 March, Toulouse, France*

Kaplan S R 2003 Private communication with the authors

Kibble B P, Rayner G H 1984 *Coaxial AC bridges* (Adam Hilger Ltd)

Pratt J R, Smith D T, Newell D B, Kramar J A, Whitenton E 2004 Progress towards Systeme International d'Unites traceable force metrology for nanomechanics *J. Mat. Res.* **19** 366-379

Reilly S P, Leach R K 2004 Review of vibration isolation techniques for use with the NPL low force balance project *to be published*

Robinson I A, Kibble B P 1997 The NPL moving-coil apparatus measuring Plank's constant and monitoring the kilogram *IEE Trans. Instrum. Meas.* **46** 596-600